ACS APPLIED MATERIALS & INTERFACES

Research Article

www.acsami.org

Surface Modification of a ZnO Electron-Collecting Layer Using Atomic Layer Deposition to Fabricate High-Performing Inverted Organic Photovoltaics

Kwang-Dae Kim,[†] Dong Chan Lim,*[,‡] Jinhee Hu,[‡] Jung-Dae Kwon,[‡] Myung-Geun Jeong,[†] Hyun Ook Seo,[†] Joo Yul Lee,[‡] Ka-Young Jang,[‡] Jae-Hong Lim,[‡] Kyu Hwan Lee,[‡] Yongsoo Jeong,[‡] Young Dok Kim,*[,†] and Shinuk Cho*[,§]

[†]Department of Chemistry, Sungkyunkwan University, Suwon, 440-746, South Korea

[‡]Surface Technology Division, Korea Institute of Materials Science, Changwon, 642-831, South Korea

[§]Department of Physics and EHSRC, University of Ulsan, Ulsan, 680-749, South Korea

Supporting Information

ABSTRACT: A ripple-structured ZnO film as the electron-collecting layer (ECL) of an inverted organic photovoltaic (OPV) was modified by atomic layer deposition (ALD) to add a ZnO thin layer. Depositing a thin ZnO layer by ALD on wet-chemically prepared ZnO significantly increased the short-circuit current (J_{sc}) of the OPV. The highest power conversion efficiency (PCE) of 7.96% with J_{sc} of 17.9 mA/cm^2 was observed in the inverted OPV with a 2-nm-thick ALD-ZnO layer, which quenched electron−hole recombination at surface defects of ZnO ripples. Moreover, an ALD-ZnO layer thinner than 2 nm made the distribution of electrical conductivity on the ZnO surface more uniform, enhancing OPV performance. In contrast, a thicker ALD-ZnO layer (5 nm) made the two-dimensional distribution of electrical conductivity on the ZnO surface more heterogeneous, reducing the PCE. In addition, depositing an ALD-ZnO thin layer enhanced OPV stability and initial performance. We suggest that the ALD-ZnO layer thickness should be precisely controlled to fabricate high-performing OPVs.

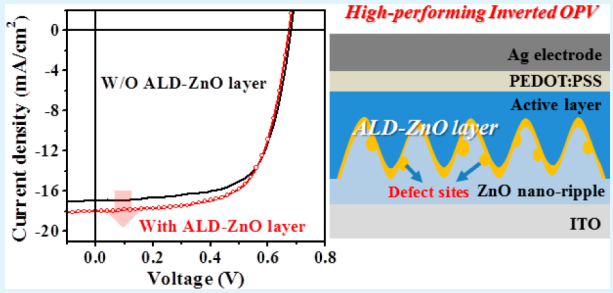

KEYWORDS: *OPV, ZnO, ALD, defects, stability*

INTRODUCTION

Solar light has garnered considerable interest as an energy source due to its renewable and environmentally friendly nature.[1,2] Among the various energy devices using solar light, organic photovoltaics (OPVs) have attracted attention due to their potential for low-cost fabrication, simple processing, lightweight, and flexibility.[1−8] There have been various efforts to fabricate high-performing OPVs, and recently, the power conversion efficiency (PCE) of OPVs exceeded 8−9% by using conjugated polymers with a low-band gap as the donor for the active layer.[9−11] Additionally, developing various types of buffer layers is important to achieve high-performance OPVs.

Buffer layers, located between the active layer and electrodes in photovoltaic devices, have been used for efficient charge separation of the electron−hole pair (exciton) generated in the active layer. The buffer layers can act as either electron- or hole-collecting (selective) layers. n-type metal oxides, such as ZnO and TiO_x, have been used as electron-collecting (selective) layers (ECLs),[12,13] whereas p-type metal oxides, such as NiO, MoO_3, WO_3, and polymer-based materials such as poly (3,4-ethylene dioxylene thiophene):polystyrene sulfonic acid (PEPOT:PSS), have been used as hole-collecting (selective) layers (HCLs).[14−16]

A nanostructure based on PEDOT:PSS as the HCL have recently shown potential to alter the optical performance and therefore increase the PCEs of OPV.[17] Also among the ECLs investigated so far, ZnO has attracted much attention due to its outstanding electrical properties, high optical transparency in the visible light range, and possibility for easy nanostructuring.[18−20] Various three-dimensional (3D) nanostructures, such as nanoripples, -wires, and -rods, of ZnO have been prepared to improve OPV performance.[18,19,21,22] The surface contact area between ZnO and the active layer can be increased by fabricating 3D ZnO nanostructures instead of 2D structures, resulting in effective electron collection from the active layer. However, many defects (e.g., oxygen vacancies), which can allow electrons and holes generated in the active layer to recombine, can form on the surface of ZnO 3D nanostructures.[23−25] Moreover, the stability of OPVs depends on the

Received: June 21, 2013
Accepted: August 16, 2013
Published: August 16, 2013

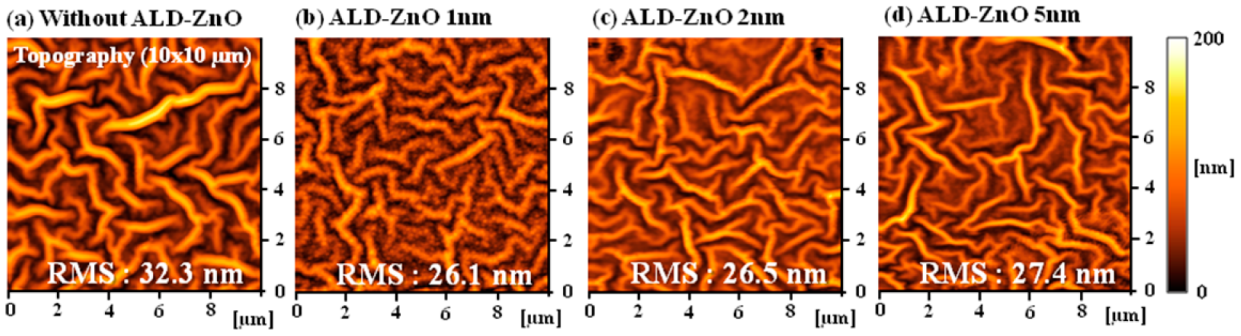

Figure 1. AFM images (10 μm × 10 μm) of ZnO nanoripple films with or without ALD-ZnO layers of various thicknesses. The ALD-ZnO layers deposited on ZnO nanoripple films were 0, 1, 2, and 5 nm thick for parts a–d, respectively.

surface-defect density of the ZnO electron transport layer.[26] ZnO surface defects can lead to degradation of the active polymer at the interface between the ZnO surface and the active layer. This degradation can reduce the PCE and stability of photovoltaic devices. Therefore, minimizing surface defects in ZnO 3D nanostructures is important to fabricate high-performing and stable photovoltaic devices.

Since atomic layer deposition (ALD) is based on the self-limiting nature of layer-by-layer growth, it can produce homogeneous films with thickness control in the subnanometer scale.[27,28] Hence, this technique is suitable for modifying the surfaces of highly complex, 3D nanostructures (e.g., such as nanoripples, -wires, and -rods). Previously, we determined that decreasing the defect density on the ZnO ECL by depositing an additional ALD layer can quench electron–hole recombination, enhancing OPV performance.[6,26] The electrical and optical properties of the ZnO film can be changed by adding an ALD layer, altering OPV performance. Therefore, ZnO film properties should be more systematically investigated as a function of the thickness of the ALD-ZnO layer to understand the relationship between ZnO ECL properties and OPV device performance. In this study, we used ZnO ripple-structures as the ECL of inverted OPVs. The active layer was a mixture of poly(thienothiophene-*co*-benzodithiophenes) 7 F-20 (PTB7-F20):$PC_{71}BM$ (8:12 mg). The ZnO ripple was created by using a sol–gel method combined with controlled heating. The surface of the ripple-structured ZnO was modified using ALD, and the relationship between OPV performance and physical ECL properties was studied by using various ECLs with different ALD-ZnO thicknesses.

RESULTS AND DISCUSSION

Figure 1 shows atomic force microscopy (AFM) images of ripple-structured ZnO films with and without additional ALD-ZnO layers of various mean thicknesses (1, 2, and 5 nm). ZnO islands grew for ALD-ZnO layers with a mean thickness of 1 nm. Ideally, ALD deposits a thin film layer by layer. However, the initial growth mechanism of thin films depends on the structure of substrate and interaction between the precursor and substrate. On heterogeneous surfaces, deposited materials can preferentially nucleate at substrate defects such as oxygen vacancies or grain boundaries. This nucleation can produce 3D islands based on the Volmer–Weber growth mechanism, as is clear in the AFM image of 1-nm-thick ALD-ZnO layers (Figure 1).[29] With increasing ALD-ZnO thickness, the ZnO islands can grow laterally to form a 2D, continuous film. When 5 nm of ALD-ZnO was deposited, the ZnO nanoripple film was almost fully covered by the ALD-ZnO layer. The root-mean-square (RMS) roughness of the ZnO surface did not change significantly with increasing thickness of the ALD-ZnO layer.

Inverted OPVs were fabricated using various ZnO nanoripple films with or without additional ALD-ZnO layers, as shown in Figure 1. The photovoltaic performances of these devices are summarized in Table 1. Devices without an ALD-ZnO layer had a PCE of 7.66% with a short-circuit current (J_{sc}) of 16.9 mA/cm^2. When the ALD-ZnO layer was deposited, the J_{sc} value increased significantly. In particularly, a device with a 2 nm-thick ALD-ZnO layer had the highest PCE of 7.96%, although it had slight decreases in the fill-factor (FF) and open-circuit voltage (V_{oc}) with respect to devices without ALD-ZnO. In contrast, a 5-nm ALD-ZnO layer resulted in lower photovoltaic performance than the 2-nm ALD-ZnO. Figure S1 in the Supporting Information summarizes the PCEs of various OPVs with ALD-ZnO layers of different thicknesses. The performance was determined for 2–3 separate OPV devices for each ALD-ZnO thickness. The PCE gradually increased as the thickness of the ALD-ZnO layer increased from 0 to 2 nm. In contrast, the PCE for 5-nm ALD-ZnO layers was lower than that for bare ZnO.

Table 1. Photovoltaic Performance of Inverted OPVs Consisting of ZnO Nano-Ripple Films with or without the ALD-ZnO Layers Described in Figure 1a–d

device description	PCE %	FF	V_{oc} (V)	J_{sc} (mA/cm^2)
W/O ALD-ZnO	7.66(±0.27)	0.665	0.679	16.9
ALD-ZnO 1 nm	7.83(±0.07)	0.655	0.668	17.9
ALD-ZnO 2 nm	7.96(±0.27)	0.659	0.672	17.9
ALD-ZnO 5 nm	7.55(±0.40)	0.616	0.680	18.0

To determine why the 2 nm ALD-ZnO layer improved photovoltaic performance, optical, structural, and electrical properties of the ZnO films in Figure 1 were characterized. In photoluminescence (PL) spectra (Figure 2), ZnO generally has two emissions peaks, a near band-edge emission at ~390 nm, and a deep level emission by surface defects (e.g., oxygen vacancies) at 530 nm.[23−25] PL spectra of ZnO were normalized by the emission intensity of the near band-edge at ~390 nm. The PL intensity at 530 nm, corresponding to surface defects on the ZnO nanoripple film, significantly decreased with increasing thickness of the ALD-ZnO layer. Therefore, as the ALD-ZnO layer grew, it gradually repaired surface defects.

In our OPV devices, the bound electron–hole pair (exciton) was photoinduced at the active layer, and the ZnO adjacent to active layer was an ECL to effectively separate the electron and hole. However, the electron and hole can recombine at ZnO

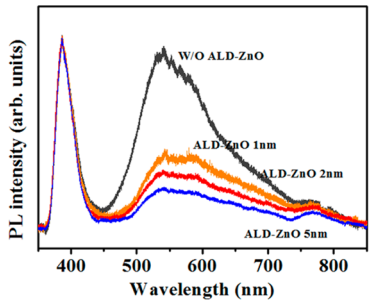

Figure 2. PL spectra of ZnO nanoripple films with or without ALD-ZnO layers described in Figure 1 (a–d). These spectra were normalized to the emission intensity of a near band-edge at ~390 nm.

surface defects, such as oxygen vacancies, reducing the photocurrent of the device.[23−25] The concentration of surface defects can be reduced by depositing an ALD-ZnO layer, enhancing the J_{sc} of the device. Therefore, depositing a 2-nm ALD-ZnO could enhance OPV performance. However, why 5-nm ALD-ZnO had a lower PCE than a 2-nm ALD-ZnO is still not clear.

Figure 3 shows ultraviolet photoelectron spectroscopy (UPS) data of various ZnO surfaces together with their work functions

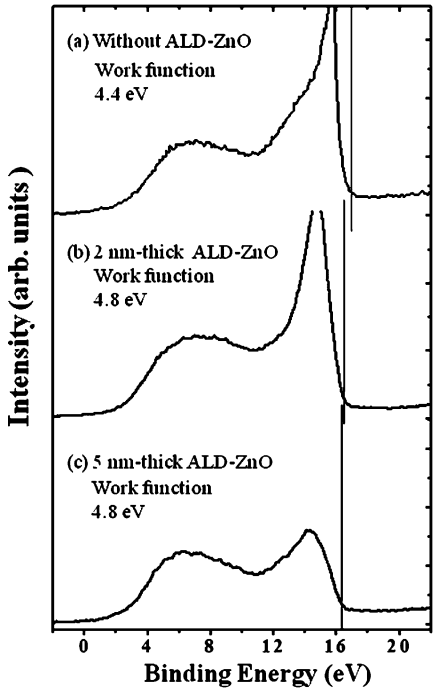

Figure 3. UPS spectra of ZnO nanoripple films with or without the ALD-ZnO layers described in Figure 1a,c, d.

determined by the energy positions of the lowest binding energy onsets of the secondary electrons. There was almost no change in the electron density at the upper part of the valence state, and only the onset position of the secondary electrons changed as a function of ALD-ZnO thickness. The work function of the ZnO surface increased from 4.4 to 4.8 eV with a 2-nm ALD-ZnO. The ZnO band shifted down as the 2-nm ALD-ZnO covered the ZnO ripples. Increasing the ALD-ZnO thickness to 5 nm caused no further significant change in the work function. The surface work function depends on the defect density and distribution and surface roughness. Therefore, the work function of the surface can change as a function of the ALD-ZnO layer. Electron extraction from phenyl-C_{71}-butyric acid methyl ester ($PC_{71}BM$) should have become less facile as the work function of the ZnO increased from 4.4 to 4.8 eV.[6] On the basis of UPS data, the increased photovoltaic performance due to the 2-nm ALD-ZnO and the differences in OPVs with 2- and 5-nm ALD-ZnO layers are not clearly understood.

Figure 4 shows results of conductive AFM of various ZnO surfaces. The topography images did not change significantly as a function of ALD-ZnO thickness, as shown in Figure 1. In contrast to the topographical images, ALD-ZnO deposition changed the current mapping images with line-profile. As the ALD-ZnO thickness increased, the current RMS of the ZnO surface decreased and then increased. The 2-nm ALD-ZnO layer had the lowest current RMS (1.78×10^{-3} nA) among the various films observed. When the ZnO nanoripple film was covered by a 5-nm ALD-ZnO layer, the current RMS again increased.

The RMS current shows how evenly electrical conductivity is distributed on the surface.[30,31] A lower RMS current implies that the surface electrical conductivity is more uniformly distributed. As the ALD-ZnO layer increased from 0 to 2 nm thickness, the current RMS decreased. The 5-nm ALD-ZnO layer had worse current uniformity than the 2-nm ALD-ZnO surface. A 1- or 2-nm ALD-ZnO layer decreased the mean conductivity of ZnO surface, whereas a 5-nm ALD-ZnO layer increased mean conductivity significantly. Conductivity may have changed as a function of ALD-ZnO thickness because during initial ALD-ZnO deposition (1 and 2 nm mean film thickness), ZnO islands repair oxygen vacancies of the ZnO-ripple increasing the 2D uniformity of conductivity. As the ALD-ZnO thickness increases, ZnO islands grow laterally, and 5-nm ALD-ZnO layers have grain boundaries between ZnO islands.[32] These grain boundaries could increase conductivity.[32,33]

The 5-nm ALD-ZnO had the lowest defect density in the PL spectrum but the highest overall conductivity and heterogeneity of conductivity. PL peak intensities between 500 and 700 nm can be considered proportional to the number of defects, as is the ZnO surface conductivity. However, our results are contrary to this simple expectation. One possible explanation for our results is that single oxygen vacancies on ZnO do not actually increase conductivity much, but groups of defects can enhance the conductivity. A 1- or 2-nm ZnO film could have a higher density of oxygen vacancies, but if they are evenly distributed on the surface it would lower conductivity. In contrast, there could be fewer, but more concentrated, oxygen vacancies on 5-nm ALD-ZnO resulting in higher heterogeneity in conductive AFM images.

The conductive AFM data reconcile OPV performance; as the uniformity of the conductivity of ZnO increased and mean conductivity decreased, the OPV performance increased. Upon depositing a 1- or 2-nm ALD-ZnO layer, ZnO oxygen vacancies, which can act as recombination centers for electrons and holes, could be repaired, increasing OPV performance. Upon depositing a 5-nm ALD-ZnO layer, defects concentrating at ZnO grain boundaries could reduce OPV performance, since these concentrated defects are most likely more efficient recombination centers than individual defects highly dispersed on the ZnO surface. Therefore, 5-nm ALD-ZnO reduced OPV performance compared to thinner ALD-ZnO layers.

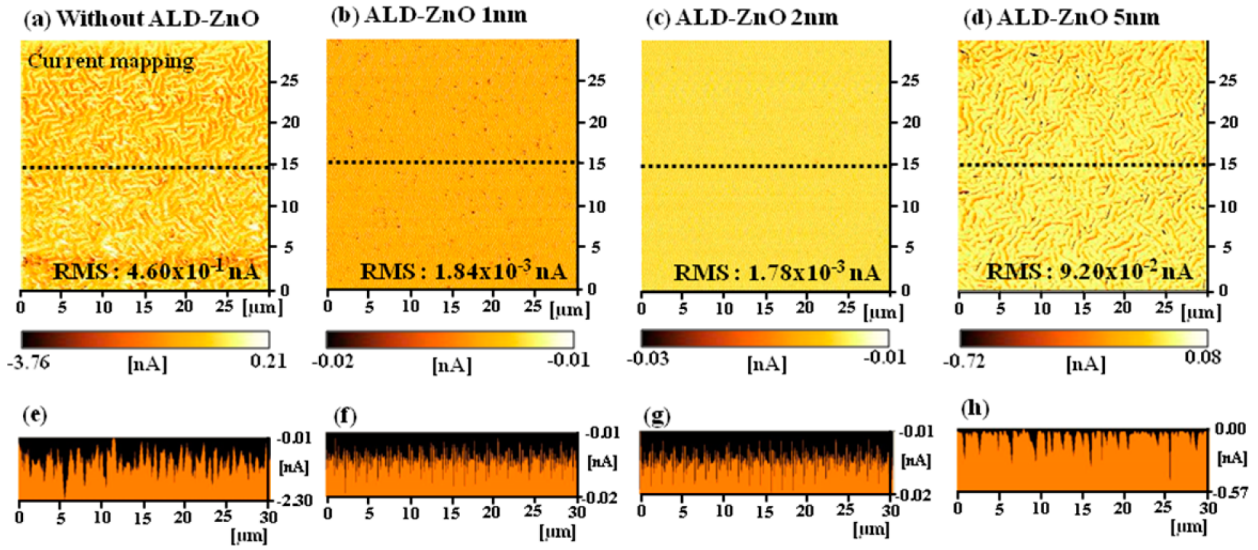

Figure 4. Current mapping (a–d) and line-profile (e–h) images (30 μm × 30 μm) analyzed by conductive AFM of different ALD-ZnO thicknesses.

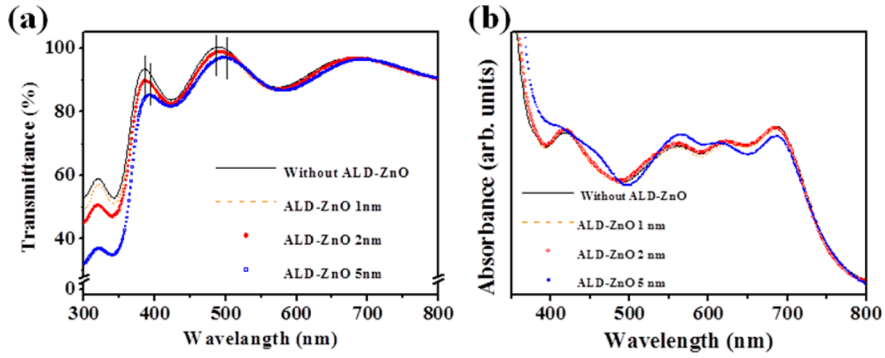

Figure 5. (a) Transmittance of ZnO nanoripple films with or without the ALD-ZnO layers described in Figure 1a–d. (b) Absorbance results of the inverted OPV in Table1.

We also measured the transmittances of ZnO nanoripple films with the ALD-ZnO layers described in Figure 1 (Figure 5a). All ZnO films exhibited high optical transmittances, above 80%, in the visible light range, as shown in Figure 5. However, when the ALD-ZnO layer thickness increased, the transmittance spectra shifted to higher wavelength and the transmittance decreased slightly. When a 5-nm ALD-ZnO layer was deposited on the ZnO nanoripple film, the transmittance pattern red-shifted by about 15 nm.

Figure 5b shows the absorbance of inverted OPVs consisting of various ZnO films with and without ALD-ZnO layers. A 2-nm ALD-ZnO layer caused no significant change in the optical absorbance compared to no ALD-ZnO layer. In contrast, a 5-nm ALD-ZnO layer changed the absorbance pattern of the donor polymer, decreasing the absorbance at 620–700 nm and increasing the absorbance at ~450 and ~570 nm. Overall, the changes in the optical properties of the OPV device as a function of ALD-ZnO thickness were not as significant as the changes in electrical properties.

External quantum efficiencies (EQEs) of inverted OPVs with a ZnO nanoripple film with and without an ALD-ZnO layer are compared in Figure 6. The EQEs of devices with thin ALD-ZnO layers (1 and 2 nm thick) were increased in a broader wavelength range (400–700 nm) than in devices without an ALD-ZnO layer. This result agrees with previous results that thin ALD-ZnO layers can increase the performance of inverted

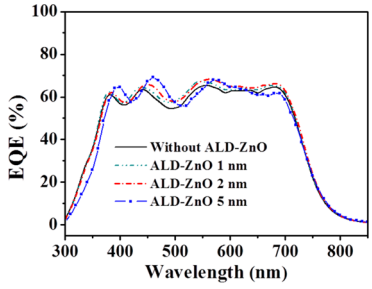

Figure 6. EQE results of the inverted OPV in Table1.

OPV by decreasing surface defects in the ZnO and more uniformly distributing surface defects. In contrast, when the ALD-ZnO layer became too thick (~5 nm), the EQE value decreased at 620–700 nm. At ~450 and ~570 nm, a 5-nm ALD-ZnO layer increased the EQE value. Overall, the change in EQE due to a 5-nm ALD-ZnO layer was analogous to the change in absorbance. A 5-nm ALD-ZnO seems to change the optical electric field of incident light induced, changing both the absorbance pattern of the active layer and the EQE of the OPV. The J_{sc} value of each OPV device can also be estimated by the EQE, and the trend in EQE as a function of ALD-ZnO thickness agrees with the J_{sc} values in Table 1 (Figure S2 in the Supporting Information).

dx.doi.org/10.1021/am402403x | ACS Appl. Mater. Interfaces 2013, 5, 8718–8723

To shed light on the stability of these devices, the photovoltaic performances of the devices with and without a thin ALD-ZnO layer (2 nm) were measured after 179 days without encapsulation (Figure 7 and Table S1 in the

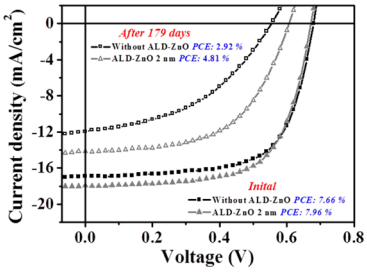

Figure 7. Photovoltaic performances of the rippled ZnO surface with or without ALD-ZnO layers (2 nm) before and after 179 days.

Supporting Information). Compared to the initial performances, PCE, J_{sc}, V_{oc}, and FF for both devices were reduced after 179 days. For the device with an ALD-ZnO layer, these values became 4.81%, 14.2 mA/cm^2, 0.606 V, and 0.559, respectively, whereas for the device without ALD-ZnO, these values decreased to 2.92%, 12.0 mA/cm^2, 0.554 V, and 0.440, respectively. The photovoltaic device with ALD-ZnO performed significantly better than the device without ALD-ZnO after 179 days. The PCE of device with ALD-ZnO was 60% of the initial PCE, whereas the PCE of the device without ALD-ZnO was 38%. This result implies that the decrease in photovoltaic performance over time of a device with an ALD-ZnO thin layer was much less pronounced than the decrease in performance of a device without ALD-ZnO. Thus, not only initial performance but also the stability of OPVs could be improved by depositing a ALD-ZnO thin layer.

CONCLUSIONS

ALD-ZnO layers were deposited on ZnO nanoripple films used as ECLs to improve the performance of an inverted OPV. The 1- and 2-nm ALD-ZnO layers enhanced OPV performance, whereas the 5-nm layers had negative effects on the OPV performance. Using various characterizations of ALD-ZnO layers, the following conclusions can be drawn regarding the basis of enhanced OPV performance by thin ALD-ZnO layers: (i) The work functions of ZnO surfaces after depositing 2- and 5-nm ALD-ZnO layers were almost identical; therefore, the work function does not indicate the basis for enhanced OPV performance by 2-nm ALD-ZnO layers. (ii) PL data show that number of oxygen vacancies gradually decreased as the mean thickness of the ALD-ZnO layer increased. This result does not agree with the OPV performance change, which increased then decreased as a function of ALD-ZnO from 0 to 5 nm. (iii) Conductive AFM measurements showed that 1- and 2-nm ALD-ZnO increased the lateral uniformity of the conductivity, whereas 5-nm ALD-ZnO decreased uniformity. Overall ZnO conductivity decreased with 1- and 2-nm ALD-ZnO layers; however, the conductivity increased with a 5-nm ALD-ZnO layer. Considering the 3D growth mechanism of ALD-ZnO layers, boundaries between the ALD-ZnO grains could be formed as the mean ALD-ZnO thickness reached 5 nm. These grain boundaries could be detrimental to OPV performance. These grain boundaries have a high local density of oxygen vacancies that could possibly act as efficient recombination centers for electrons and holes in actual OPV devices.

Additionally, the photovoltaic performance of devices with and without ALD-ZnO layers was measured after 179 days without any encapsulation to determine the stability of these devices. Devices with an ALD-ZnO layer not only had enhanced initial performance but also significantly higher stability than devices without ALD-ZnO. We suggest that the thickness of an ALD-ZnO layer should be precisely controlled to fabricate a high-performance OPV and that the ALD technique is a suitable method to control the thickness.

EXPERIMENTAL SECTION

The inverted OPV consisted of a stack of indium tin oxide (ITO)-coated glass/ZnO nanoripple film with or without an ALD-ZnO layer/bulk heterojunction of donor and acceptor polymer as an active layer/PEDOT:PSS/Ag top-electrode. The ITO-coated glass substrates (4 Ω/sq, 2.5 × 2.5 cm^2) used as the transparent electrode were cleaned with distilled water, ultrasonicated in acetone and boiling isopropyl alcohol, and dried in a 100 °C oven. To prepare a ZnO nanoripple film, 0.75 M ZnO sol−gel solution was spin-coated on ITO-coated glass pretreated with UV-ozone for 30 min. The solution was prepared by dissolving zinc acetate [$Zn(CH_3COO)_2{\cdot}2H_2O$] in 2-methoxyethanol solvent containing ethanolamine as a stabilizer. After coating, the glass was heated to 350 °C with a constant heating rate of 22 °C/min in a furnace. The details of the synthesis and effects of the ZnO nanoripple film have been reported elsewhere.[21]

To prepare the active layer, a mixture of poly(thienothiophene-*co*-benzodithiophenes) 7 F-20 (PTB7-F20):$PC_{71}BM$ (8:12 mg) was dissolved in 1 mL of chlorobenzene with 3% (v/v) 1,8-diiodooxtane (Aldrich) with stirring overnight at 60 °C. This solution was spin-coated on ZnO nanoripple films under Ar at room temperature (1000 rpm/40 s).

The ZnO film surface was further modified using an ALD system (LUCIDA M100, NCD). Diethyl zinc [DEZ, $Zn(C_2H_5)_2$] and water (H_2O) vapor were used as the zinc precursor and reactant, respectively. The DEZ source was maintained at 10 °C using a cooling circulator. The canister containing the water source was at room temperature. During deposition, Ar gas was continuously supplied to the reaction chamber at a flow rate of 100 sccm. ZnO-ALD was deposited at 1.39 Å/cycle. To grow ZnO layers 1, 2, and 5 nm thick, 7, 14, and 36 ALD cycles were used, respectively.

The PEDOT:PSS (Clevios P VP AI 4083, Heraeus) used as a hole injection layer was diluted in isopropyl alcohol (IPA). A PEDOT:PSS/IPA mixture (1:10 volume ratio) was spin-coated onto the active layer under Ar at room temperature (5000 rpm/60 s). No post annealing of the PEDOT:PSS layers was used.

The Ag metal (100 nm) top electrode was thermally evaporated onto the PEDOT:PSS layer under 3 × 10^{-6} Torr. The active surface area of the device with the metal mask was 0.38 cm^2.

The current density−voltage (J−V) curves of the OPV devices were taken using a PEC-L11 model 13 (Pecell Technologies Inc.) under AM 1.5 simulated illumination of 100 mW/cm^2. The intensity of sunlight illumination was calibrated using a standard Si-photodiode detector with a KG-5filter. EQE spectra of each OPV were obtained by using a solar cell spectral response/QE/IPCE measurement system (Newport Co., Oriel IQE-200TM).

The structures and electrical properties of ZnO nanoripple films with and without ALD-ZnO thin layers were analyzed by conductive AFM consisting of a current-sensing module. The AFM was operated in contact mode with rate 0.3 Hz using the Pt-coated cantilever tips (diameter, 15−20 nm) from Nanosensors, Switzerland (spring constant of 3 N/m and resonance frequency of 75 kHz) to produce topographic and current images of the sample surface. A bias voltage between the sample electrode (ITO) and the conducting cantilever tip (which was grounded) was 10 V during all experiments. The c-AFM setup allowed current measurements to 100 fA (minimum value).

To measure optical properties, PL and UV/vis spectrometers were used. PL spectra were measured using a HORIBA JOBIN YVON, LabRam HR800. Samples were pumped with a He−Cd laser of

wavelength of 325 nm. Transmittance and absorption spectra were obtained from Varian, Cary5000 UV/vis spectrometer.

For UPS studies, an ultrahigh vacuum system with a base pressure of 3×10^{-10} Torr equipped with a concentric hemispherical analyzer was used. He I was used as the UV source.

■ ASSOCIATED CONTENT

Ⓢ Supporting Information

Additional figures showing PCEs of various OPVs as a function of ALD-ZnO thickness, J_{sc} value estimated by the EQEs, and a table summarizing photovoltaic performance before and after 179 days. This material is available free of charge via the Internet at http://pubs.acs.org.

■ AUTHOR INFORMATION

Corresponding Authors

*Phone: ++82 55 280 3511. Fax: ++82 55 280 3570. E-mail: dclim@kims.re.kr (D.C.L.).

*Phone: ++82 31 299 4564. Fax: ++82 31 290 7075. E-mail: ydkim91@skku.edu (Y.D.K.).

*Phone: ++82 52 259 1268. Fax: ++82 52 259 2327. E-mail: sucho@ulsan.ac.kr (S.C.).

Notes

The authors declare no competing financial interest.

■ ACKNOWLEDGMENTS

This research was supported by the Korea Institute of Materials Science (KIMS).

■ REFERENCES

(1) Yu, G.; Gao, J.; Hummelen, J. C.; Wudl, F.; Heeger, A. J. *Science* **1995**, *270*, 1789−1791.

(2) Wienk, M. M.; Kroon, J. M.; Verhees, W. J. H.; Knol, J.; Hummelen, J. C.; van Hal, P. A.; Janssen, R. A. J. *Angew. Chem.* **2003**, *115*, 3493−3497.

(3) Peet, J.; Heeger, A. J.; Bazan, G. C. *Acc. Chem. Res.* **2009**, *42*, 1700−1708.

(4) Yang, X.; Loos, J.; Veenstra, S. C.; Verhees, W. J. H.; Wienk, M. M.; Kroon, J. M.; Michels, M. A. J.; Janssen, R. A. J. *Nano Lett.* **2005**, *5*, 579−583.

(5) Nelson, J. *Mater. Today* **2011**, *14*, 462−470.

(6) Lim, D. C.; Kim, K.-D.; Park, S.-Y.; Hong, E. M.; Seo, H. O.; Lim, J. H.; Lee, K. H.; Jeong, Y.; Song, C.; Lee, E.; Kim, Y. D.; Cho, S. *Energy Environ. Sci.* **2012**, *5*, 9803−9807.

(7) Gunes, S.; Neugebauer, H.; Sariciftci, N. S. *Chem. Rev.* **2007**, *107*, 1324−1338.

(8) Li, G.; Zhu, R.; Yang, Y. *Nat. Photon.* **2012**, *6*, 153−161.

(9) He, Z.; Zhong, C.; Su, S.; Xu, M.; Wu, H.; Cao, Y. *Nat. Photon.* **2012**, *6*, 591−595.

(10) Dou, L.; You, J.; Yang, J.; Chen, C.-C.; He, Y.; Murase, S.; Moriarty, T.; Emery, K.; Li, G.; Yang, Y. *Nat. Photon.* **2012**, *6*, 180−185.

(11) Yang, T.; Wang, M.; Duan, C.; Hu, X.; Huang, L.; Peng, J.; Huang, F.; Gong, X. *Energy Environ. Sci.* **2012**, *5*, 8208−8214.

(12) Lim, F. J.; Ananthanarayanan, K.; Luther, J.; Ho, G. W. *J. Mater. Chem.* **2012**, *22*, 25057−25064.

(13) Liang, Z. Q.; Zhang, Q. F.; Wiranwetchayan, O.; Xi, J.; Yang, Z.; Park, K.; Li, C. D.; Cao, G. Z. *Adv. Funct. Mater.* **2012**, *22*, 2194−2201.

(14) Steirer, K. X.; Chesin, J. P.; Widjonarko, N. E.; Berry, J. J.; Miedaner, A.; Ginley, D. S.; Olson, D. C. *Org. Electron.* **2010**, *11*, 1414−1418.

(15) Yang, T.; Wang, M.; Cao, Y.; Huang, F.; Huang, L.; Peng, J.; Gong, X.; Cheng, S. Z. D.; Cao, Y. *Adv. Energy Mater.* **2012**, *2*, 523−527.

(16) Lee, J.-S.; Jang, I.-H.; Park, N.-G. *J. Phys. Chem. C* **2012**, *116*, 13480−13487.

(17) Meier, R.; Birkenstock, C.; Palumbiny, C. M.; Müller-Buschbaum, P. *Phys. Chem. Chem. Phys.* **2012**, *14*, 15088−15098.

(18) Yang, T.; Sun, K.; Liu, X.; Wei, W.; Yu, T.; Gong, X.; Wang, D.; Cao, Y. *J. Phys. Chem. C* **2012**, *116*, 13650−13653.

(19) Choi, H. W.; Lee, K.-S.; Alford, T. L. *Appl. Phys. Lett.* **2012**, *101*, 153301-1−4.

(20) Zhang, Q.; Dandeneau, C. S.; Zhou, X.; Cao, G. *Adv. Mater.* **2009**, *21*, 4087−4108.

(21) Lim, D. C.; Shim, W. H.; Kim, K.-D.; Seo, H. O.; Lim, J.-H.; Jeong, Y.; Kim, Y. D.; Lee, K. H. *Sol. Energy Mater. Sol. Cells* **2011**, *95*, 3036−3040.

(22) Zhang, Q.; Yodyingyong, S.; Xi, J.; Myers, D.; Cao, G. *Nanoscale* **2012**, *4*, 1436−1445.

(23) Irimpan, L.; Nampoori, V. P. N.; Radhakrishnan, P.; Deepthy, A.; Krishnan, B. *J. Appl. Phys.* **2007**, *102*, 063524-1−6.

(24) Layek, A.; Manna, B.; Chowdhury, A. *Chem. Phys. Lett.* **2012**, *539*−*540*, 133−138.

(25) Seo, H. O.; Park, S.-Y.; Shim, W. H.; Kim, K.-D.; Lee, K. H.; Jo, M. Y.; Kim, J. H.; Lee, E.; Kim, D.-W.; Kim, Y. D.; Lim, D. C. *J. Phys. Chem. C* **2011**, *115*, 21517−21520.

(26) Park, S.-Y.; Seo, H. O.; Kim, K.-D.; Lee, J. E.; Kwon, J.-D.; Kim, Y. D.; Lim, D. C. *Phys. Status Solidi R* **2012**, *6*, 196−198.

(27) George, S. M. *Chem. Rev.* **2009**, *110*, 111−131.

(28) Bakke, J. R.; Pickrahn, K. L.; Brennan, T. P.; Bent, S. F. *Nanoscale* **2011**, *3*, 3482−3508.

(29) Argile, C.; Rhead, G. E. *Surf. Sci. Rep.* **1989**, *10*, 277−356.

(30) Tkalya, E.; Ghislandi, M.; Alekseev, A.; Koning, C.; Loos, J. *J. Mater. Chem.* **2010**, *20*, 3035−3039.

(31) Lee, H. J.; Lee, J.; Park, S.-M. *J. Phys. Chem. B* **2010**, *114*, 2660−2666.

(32) Lin, H.-J.; Lin, D.-Y.; Hong, J.-Z.; Yang, C.-S.; Lin, C.-M.; Lin, C.-F. *Phys. Status Solidi C* **2009**, *6*, 1468−1471.

(33) Winston, R. A.; Cordaro, J. F. *J. Appl. Phys.* **1990**, *68*, 6495−6500.